Materials Horizons

ROYAL SOCIETY OF CHEMISTRY

COMMUNICATION

View Article Online
View Journal

Cite this: DOI: 10.1039/d5mh01817j

Received 24th September 2025,
Accepted 19th December 2025

DOI: 10.1039/d5mh01817j

rsc.li/materials-horizons

Multidimensional, multilevel information storage and encryption in auxetic liquid crystal elastomers

Zhenming Wang,[ab] Thomas Raistrick,[b] Ming Cheng,[a] Emily J. Cooper,[b] Matthew Reynolds,[b] Mengjia Cen,[a] Helen F. Gleeson *[b] and Yan Jun Liu *[a]

The rapid development of information technology comes with associated challenges in information storage and security and there is a need for new approaches that allow multilevel information storage and encryption (M^2ISE). This paper describes an innovative strategy for realizing M^2ISE in a soft material that is simply manufactured and operated. An auxetic liquid crystal elastomer film is utilized, programmed in specific regions to exhibit strain-dependent optical and morphological responses. The auxetic response is controlled by the application of chosen voltages, all $\lesssim$2.00 V_{rms}, during polymerization. The information is patterned using UV-masks that are designed to realize both 2D optical and 3D tactile information in the form of binary images and haptic Braille letters respectively. The addressing voltages are determined by measuring the elastic and dielectric properties of the precursor mixture and the auxetic strain threshold can be tuned between $\sim$0.58 $\pm$ 0.05 and $\sim$0.91 $\pm$ 0.05. The decryption processes for the optical and tactile information are independent and offer security through the need for strains of specific magnitudes and directions. This study represents an innovative approach for encryption of information utilizing a recently-discovered family of soft materials, auxetic liquid crystal elastomers.

New concepts

Information storage and encryption is an increasingly important topic and there is a need for new materials that allow both secure storage and decryption of information. In this work, we report the use of unique materials discovered in 2018, namely auxetic liquid crystal elastomers (LCEs), as an innovative approach that allows both optical and tactile information to be recorded and recovered in thin, elastomeric films. The films studied are programmed by the use of an applied voltage to define a specific director pattern during polymerization, with the desired information patterned using a UV-mask. They are read by applying specific strains to the films. The auxetic response of the elastomeric film, *i.e.* the point where it becomes thicker on strain rather than thinner, depends on the voltage applied during the polymerization. This auxetic behavior allows us to record tactile information, while a related dark state facilitates the storage of optical data. We demonstrate the recording and recovery of binary optical information and tactile Braille letters, representing a unique multidimensional and multilevel system.

1. Introduction

With the booming development of information technologies, for example artificial intelligence (AI) technology and 5G networks, we have entered a prosperous information age. The rapid transmission of information and increasing demand for information storage has a downside as there are increasing problems around false information and leakage of personal information. Information storage and security are therefore receiving tremendous attention, promoting the requirements for advanced technologies and materials for storage and encryption. In recent years, experts in different areas have made enormous efforts to explore new strategies for information storage and encryption, including metasurfaces,[1–3] photonic materials,[4–6] holograms[7–9] and fluorescent/phosphorescent imaging.[10–13] Through precise fabrication processes, the information is stored in systems that are designed to avoid replication. However, the information coding processes can be complicated, and costly equipment is generally necessary for the complex encryption process. Therefore, it is still a challenge to achieve multidimensional, multilevel information storage and encryption (M^2ISE) with techniques that involve simple material manufacturing and convenient operation.

Liquid crystal elastomers (LCEs) are polymerized soft materials with programmable and reversable deformation possible under multiple stimuli (for instance, heat,[14,15] light,[16,17] electric fields[18,19] and mechanical strain.[20,21]). Such materials have already shown great value in fields such as soft robotics,[22–24] soft actuators,[25–27] sensors[28,29] and optical devices.[30–33] As moderately cross-linked liquid crystal polymer networks composed of rigid liquid crystal molecules (mesogens) and a flexible polymer backbone network,

[a] Department of Electronic and Electrical Engineering, State Key Laboratory of Optical Fiber and Cable Manufacture Technology, and Shenzhen Engineering Research Centre for High Resolution Light Field Display and Technology, Southern University of Science and Technology, Shenzhen, 518055, China. E-mail: yjliu@sustech.edu.cn

[b] School of Physics and Astronomy, University of Leeds, Leeds, LS2 9JT, UK. E-mail: H.F.Gleeson@leeds.ac.uk

LCEs retain both the anisotropy of liquid crystals and the elasticity of a polymer network, which endows LCEs controllable optical properties and programmable shape deformations. Playing a vital role as a class of polymerized soft materials which have been explored and utilized to handle the challenges aimed at M^2ISE,[34–38] LCEs have also demonstrated their capabilities in the areas of information storage and encryption.[39–47] Such applications take advantage of LCE's controllable, often unique, optical properties and programmable shape deformations. For instance, Lagerwall's team have used the complex optical patterns formed by arrays of chiral nematic shells as unique identifiers in anti-counterfeiting markers.[39,40] In 2024 Ko's group realized high-resolution, multilevel patterning and transmittance modulation for rewritable information through laser-induced dynamic crosslinking.[41] Li and his team achieved dual-mode, multilevel information encryption and real-time, rewritable information display by modifying the chemical composition of LCEs.[42] Generally, the information encryption strategy of LCEs relies on the utilization of unique anti-counterfeiting techniques[39–47] or a combination of multiple stimuli that trigger the decryption.[43,44,46,47] The strategy for accomplishing the decryption and display of information is based on the transmittance or color change of LCEs caused by (1) intrinsic phase transitions;[41,42] (2) mesogen order or reorientation;[39,40,47] (3) phosphorescence/fluorescence[43,44,47] or (4) structural color changes.[39,45,46] Storage capacity and safety have been assured through the integration of different encryption techniques and the combination of various decryption triggers. However, the encryption processes can be complicated, and various triggers sometimes easily interfere with each other. Therefore, there is still space and opportunity for implementing easily fabricated and conveniently operated LCEs to realize M^2ISE.

In addition to their optical properties, it is worth noting that the programmable stimulus-responsive deformations of LCEs could expand the modes of information storage from 2 dimensional (2D) to 3 dimensional (3D), the latter of which could be stored as tactile information.[48–51] Nowadays, the widely used tactile displays are pin type displays which convey textual information to visually impaired people by expressing 2.5D information.[52–54] These refreshable and height-adjustable displays are generally rigid and require bulky hardware comprised of a mechanical driver and actual moving parts. Polymerized soft materials, with reversible stimulus-responsive deformations have offered new strategies for making flexible actuator-based tactile displays,[55,56] for example, Hwang *et al.* have made tactile displays assembled using a bilayer poly(*tert*-butyl acrylate) (P*t*BA)-PDMS polymer and a near-infra-red light-emitting diode array. The pneumatic pressure on each pixel is generated by a photothermal actuation, to realize a reversible and height-adjustable topological expression.[55] The programmable properties of LCEs show promise in helping tactile displays get rid of their clumsy mechanical drivers and several notable attempts have been made. Torras *et al.* fabricated a tactile display array by assembling micro-LCE-pillars in 2013.[50] Their thermally-actuated LCE array demonstrated the feasibility of LCE-based tactile displays. In 2023, Terentjev's group synthesized an LCE with millimeter-scale protruding features and realized a complete Braille dynamic display.[51] Presently, LCEs still have great potential to be tapped and developed in the aspect of multilevel tactile information storage and encryption.

In this work, we present a novel yet facile strategy that uses intrinsic auxetic liquid crystal elastomers (IALCEs) to accomplish M^2ISE for not only 2D optical information but also for 3D tactile information. We demonstrate that the auxetic response of a single IALCE material can be effectively modified and controlled by tuning alignment within the LCE film through specific, voltage-dependent alignment of the precursor mesogens during polymerization. The resulting voltage-programmed auxetic responses offer tunable optical and morphological changes of the IALCEs which can be further used to achieve M^2ISE. In this work, through polymerization under low voltages (0.9 to 2.0 V_{rms}) with exposure masks, 3-level 2D optical information (in the format of binary signals) and 3D tactile information (in the format of haptic letters using the Braille convention) respectively are selectively encrypted and stored into IALCEs at the polymerization stage. Subsequently, the multilevel information is decrypted stage-by-stage by mechanically stretching the IALCEs to pre-determined strains. The decryption processes for the 2D and 3D information do not interfere with each other and only through applying a specific strain in a defined stretching direction is the correct information shown. This work offers a new strategy for developing M^2ISE soft materials in a simply fabricated and conveniently operated way with potential applications in data storage, encryption and display systems for not only optical but also tactile information.

2. Experimental

2.1. Materials

The polyvinyl alcohol (PVA, M_w 13 000–23 000, 98%), the dichloromethane (DCM, CH_2Cl_2, 99.8%) and the methanol (CH_3OH, 97%) were all from Sigma-Aldrich, USA. The 6-(4-cyano-biphenyl-4′-yloxy)hexyl acrylate (A6OCB, $C_{22}H_{23}NO_3$, 98%), 4′-Hexyloxy-biphenyl (6OCB, $C_{18}H_{21}NO$, 98%) were ordered from Ning Cui Optics Technology Ltd., China. The 1,4-bis-[4-(6-acryloyloxyhexyloxy)benzoyloxy]-2-methylbenzene (RM82, $C_{39}H_{44}O_{10}$, 98%) were ordered from Synthon Chemical GmbH, Germany. The 2-ethylhexyl acrylate (EHA, $C_{12}H_{22}O_2$, 98%) and methyl benzoylformate (MBF, $C_9H_8O_3$, 97%) were obtained from Rhawn Chemical GmbH, China. None of the chemicals were further purified. The indium Tin oxide (ITO) glass substrates were bought from Xinyan Technology Ltd., China, and the ITO-coated polyethylene terephthalate (PET) films (ITO-PET) were purchased from Sigma-Aldrich, USA. The Melinex401 films were from Dupont Tejin film, USA.

2.2. The fabrication of 2D optical M^2ISE IALCE

The fabrication process is modified from the fabrication of IALCEs by including a mask to select areas for polymerization under specific conditions of voltage or temperature (in the isotropic case). After capillary filling the precursor into the cell and leaving the sample at room temperature to achieve good,

homogeneous alignment, an exposure mask with a 3 × 3 array of transparent 'holes' was used to code the binary pattern into the IALCE. The pixels in the array were 3 mm × 2 mm ellipses. For the first round of information coding (1), the exposed areas were polymerized under 0 V_{rms} with a 365 nm UV light at 10 mW cm^{-2} for 10 min, ensuring the full polymerization of the coded areas. After the first cycle, the cell was heated to 50 °C, held for 5 min and then left at room temperature again so that the nematic phase aligns. The second (2) and third (3) cycles of coding repeat the same process as the first round with different masks and applied voltages. After the final (4) cycle, the cell was heated to the isotropic state (50 °C) with no mask and fully polymerized with a 365 nm UV light at 10 mW cm^{-2} for 20 min. Finally, the film was peeled off and washed with a DCM solution (30% in methanol).

2.3. The fabrication of 3D tactile M²ISE IALCE

For the coding of tactile information, each film represents a separated haptic pixel. All the coding process utilized the same exposure mask, and the exposure region was an 8 mm × 5 mm ellipse. The tactile information was coded by polymerizing the exposed areas under 0 V_{rms}, 1.25 V_{rms} and 1.50 V_{rms}, separately, with a 365 nm UV light at 10 mW cm^{-2} for 10 min, and after coding, the cell was heated to 50 °C and the remaining area was fully polymerized in the isotropic phase, using 365 nm UV light at 10 mW cm^{-2} for 20 min. Finally, after the film was removed and with DCM solution (30% in methanol), the tactile film was ready for use.

2.4. Mechanical deformation measurement of IALCEs

The mechanical deformation measurement was carried out with a 5% step strain and was held for 10 min at room temperature to allow strain release for each step. The LCE film was initially 0.1 mm thick, and the stretching speed was ∼0.02 mm s^{-1}. Higher strain rates are known to increase the auxetic threshold and reduce the magnitude of the auxetic response.[57] Considering the auxetic response of the sample, to provide both a sufficiently strong magnitude and fast realisation time, we selected a strain rate of 0.5% min^{-1}. The cyclic mechanical measurement was performed using Dynamic Mechanical Analysis (TA Instruments™ DMA 850), with a setup using a series of rate-controlled strain ramps. The material was first strained to 0.85 strain, followed by 35 repeat cycles between 0.85 and 0.65 strain, at the same strain rate. All experiments were performed at room temperature.

2.5. Differential scanning calorimetry (DSC)

DSC was used to measure the glass transition temperature of the LCEs. To prepare a sample for DSC measurement, a small piece was cut from the prepared LCE film, weighed and hermetically sealed in an aluminum pan. A Q20 DSC (TA instrument, UK) with heating/cooling rates of 10 °C min^{-1} from −60 °C to 120 °C allowed the glass transition to be determined.

2.6. Surface morphology measurement

The surface morphology of the film prepared for demonstration of the tactile information was measured by a laser scanning microscope (VK-X1000, Keyence Pte. Ltd, Singapore). The instantaneous laser scanning figures were obtained with a 10× objective lens. When all the samples were stretched and strain released, a scan across the film surface gave pixel-by-pixel with a resolution of 2 × 2 mm^2. The resolution of the topological profile measurement, undertaken with the 'Anytest' software is about 0.1 mm.

3. Results and discussion

3.1. IALCE synthesis and characterization

As shown in previous studies,[20,21,58–62] the LCE synthesized using the compounds shown in Fig. 1a exhibits an intrinsic auxetic (negative Poisson's ratio) response in a direction perpendicular to both the LC orientation and the strain. During the stretching process, the nematic order changes, with uniaxial order decreasing while biaxial order emerges leading to the auxetic behaviour.[21,58,60] When the IALCEs are stretched to a certain threshold strain, ε_{Th}, the Poisson's ratio in the auxetic direction reaches zero and becomes negative upon further stretching. In this work, we used the same precursor mixture as has been previously employed but additionally applied an electric field during polymerization to induce a patterned director field in the depth of the film. The detailed fabrication process is described in the SI and the schematic is shown in Fig. 1b. Table S1 in the SI shows the proportions of the components in the precursor mixture and final IALCE sample, respectively. After polymerization, the unreactive 6OCB was washed out and IALCEs exhibited anisotropic deswelling with a dimensional contraction of ∼3% along the director and ∼30% perpendicular to the director.[32] The thickness remains almost unchanged.

Fréedericksz transition alignment is an equilibrium state that occurs when the orientation imposed on the director by surface anchoring at the cell boundaries conflicts with that of an applied external field.[63] In Fréedericksz transition alignment, the director of the liquid crystal adopts a minimum energy profile which has a maximum reorientation in the direction of the applied field at the centre of the cell that depends on the magnitude of the applied voltage (see SI for details of the calculation of the director profile for specific applied voltages). A schematic depicting the director alignment that occurs is shown in Fig. 1c. The director, depicted by the unit vector $\hat{n}$, is initially uniformly planar. When a voltage is applied above the threshold for the nematic material employed, V_{Th}, the orientation profile of the director varies continuously throughout the cell. The director is strongly anchored and effectively parallel at the substrates, with the tilt varying continuously throughout the depth of the device in a manner that depends on the precursor mixture elastic constants and applied voltage, V. At the centre of the cell the director adopts a maximum value, θ_{max}, defined by the ratio V/V_{Th} and shown in Fig. 1d. The director profile through the depth of the cell $\theta(z/d)$ has been calculated for values of θ_{max} at 5° intervals for the precursor mixture, as described in the SI and is shown in Fig. S1. It can be seen in Fig. 1d that voltages lower than $V/V_{Th} \sim 1.17$ (*i.e.* ∼1.05 V_{rms}) are in the region where the dependence of θ_{max} changes rapidly. As this might introduce significant errors into

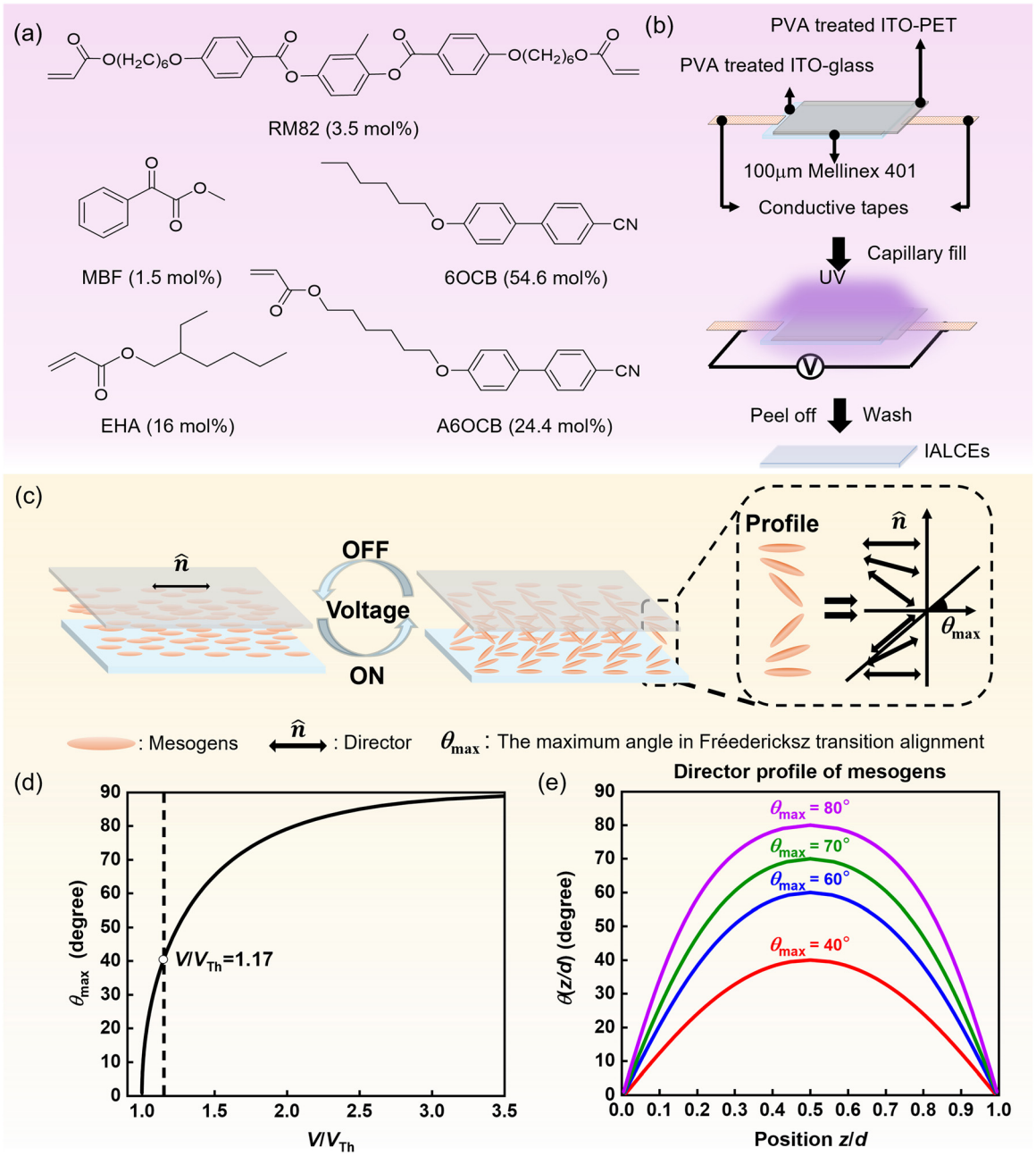

Fig. 1 (a) The molecular structures of the IALCE monomers with relative proportions for the precursor mixture indicated. (b) A cartoon depicting the fabrication of the IALCEs. The glass and polyethylene terephthalate (PET) substrates have Indium Tin Oxide (ITO) electrodes to enable the application of voltage and are coated with rubbed polyvinyl alcohol (PVA) to ensure planar alignment at the film surfaces. (c) A schematic of Fréedericksz transition alignment of the nematic director. The director is initially uniformly planar aligned in the cell with no voltage applied. When a voltage greater than V_{Th} is applied, the director reorients most in the center of the device, with a continuous profile from each surface. The orientation profile and the corresponding director orientation are shown schematically in the zoomed figure. The maximum rotation angle of the director in the middle of the cell is defined as θ_{max}. (d) The maximum angle θ_{max} of the IALCE precursor for different applied voltages, V, with respect to V_{Th}. The dotted line shows the position of $V/V_{Th} \sim 1.17$. (e) The director profiles through the cell from one substrate ($z/d = 0$) to the other ($z/d = 1$) calculated for values of θ_{max} at 40°, 60°, 70° and 80°.

the desired director profile, 1.05 V_{rms} is the minimum voltage used in this work to synthesize the IALCEs. The four voltages selected (1.05 V_{rms}, 1.25 V_{rms}, 1.50 V_{rms} and 2.00 V_{rms}) have θ_{max} values near to 40°, 60°, 70° and 80°, respectively. The director distribution throughout the cell under each of these conditions is shown in Fig. 1e. Here, we use the notation 1.05 V_{rms}-IALCE to refer to an IALCE polymerized under 1.05 V_{rms} and the same format is used to name materials that are polymerized under different voltages.

High quality alignment in the ~100 μm thick LCE films produced was verified by polarized optical microscopy (POM), Fig. S2. The glass transition temperature, T_g, of each sample

was measured and the measurement process is described in the experimental section. The glass transition temperature T_g, measured using differential scanning calorimetry (Fig. S3) was found to be 15 ± 1 °C for all films, irrespective of whether or not a voltage was applied. This is unsurprising, given that the chemical constituents and crosslink density are identical in each case but is important to note as it has been shown that the auxetic threshold strain in LCEs can depend on T_g.[60]

For every IALCE film, mechanical measurements were performed to determine the impact on the auxetic response of introducing a patterned director alignment in the depth of the film through the Fréedericksz transition in the geometry shown in Fig. 2a. It is

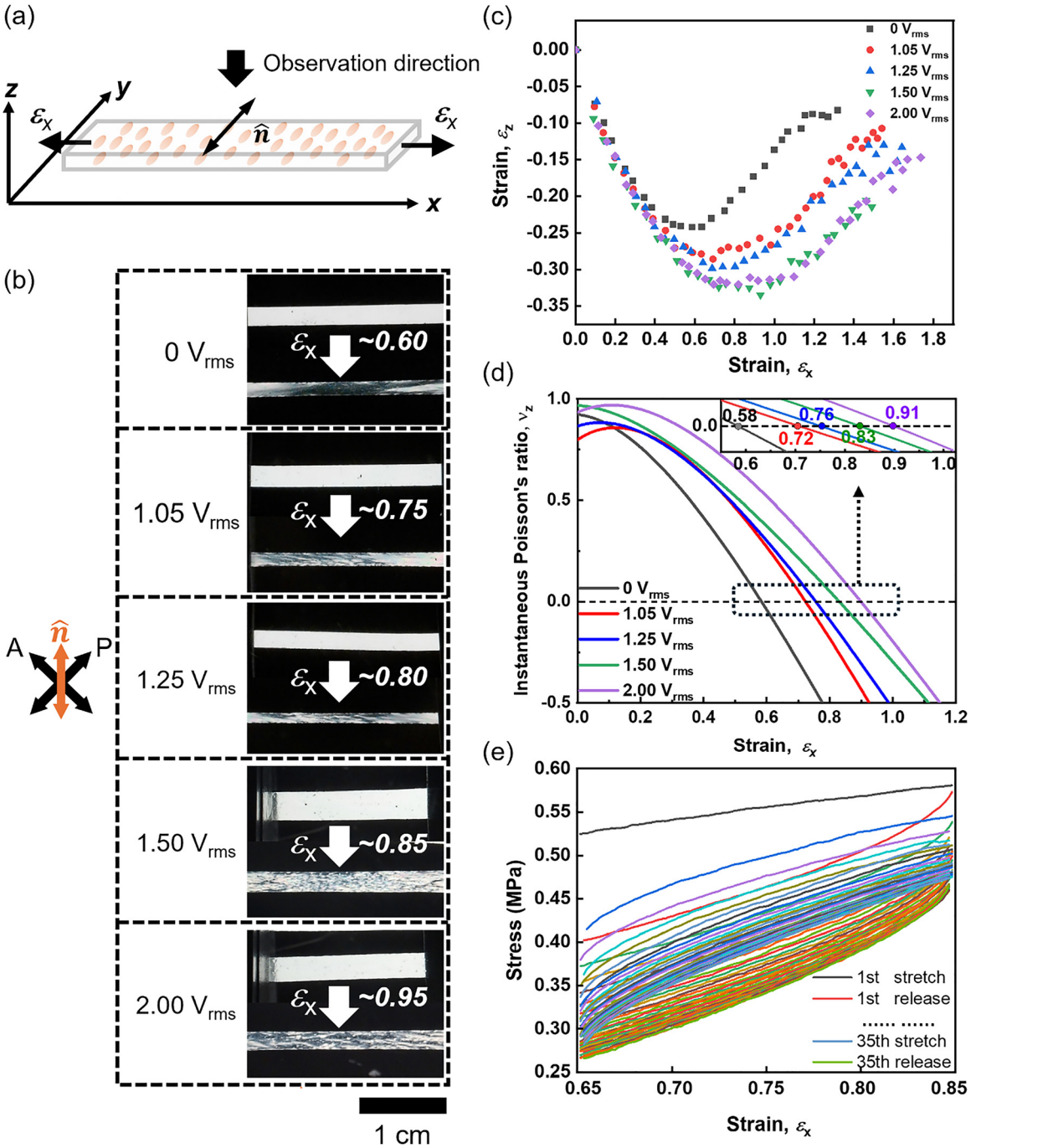

Fig. 2 (a) The geometry of the undeformed IALCE samples. The projection of the director $\hat{n}$ is parallel to the y-axis and the strain is applied along the x-direction (ε_x). The observation direction is along the z-direction. (b) The POM images show the initial, unstrained, state and the dark state emerging near the threshold auxetic strain for the IALCE prepared at 0 V_{rms}, 1.05 V_{rms}, 1.25 V_{rms}, 1.50 V_{rms} and 2.00 V_{rms}. The strains of the dark states are indicated, all of which are near though higher than the ε_{Th}. The scale bar is 1 cm. (c) The strain ε_z as a function of ε_x measured for all the samples. (d) The instantaneous Poisson's ratio in the thickness of the film, υ_z, measured for all the samples. The inset figure shows the crossing of each line at υ_z = 0. (e) The 35-cycle mechanical measurement of a planar IALCE sample.

known that when the director is orthogonal to the strain, the auxetic response occurs in a direction perpendicular to both the director and the strain, in this case along the z-direction. The emergence and growth of biaxial order in these LCEs under strain leads to both a mechanical and optical response. Auxetic behavior (negative Poisson's ratios) is observed above a threshold strain, ε_{Th} when the out-of-plane population of the mesogens associated with the biaxial response becomes sufficient to cause the film to become thicker on increasing strain. The biaxial optic axis also changes sign at a characteristic strain, causing the film to appear isotropic (dark between crossed polarizers) at a specific strain value; this is an optical signature of the auxetic behavior, though the dark state does not necessarily occur exactly at the auxetic threshold.[20] The measurements were performed on 100 mm thick films using customized equipment, described in detail elsewhere,[20,64] but briefly consisting of two clamps equipped with actuators, a tensile sensor and a loading chamber in a configuration in which a polarizing microscope optical system was integrated.[20] The apparatus allows both mechanical and optical measurements as polarized images of IALCE samples may be observed while simultaneously under strain.

Details of the mechanical measurements for each film are shown in the SI Videos S1–S5 and instantaneous images showing the initial (unstrained) film and the emergence of the optically dark state of each IALCE film are shown in Fig. 2b. The behaviours of ε_z (strain in the z-direction) and ε_y (strain in the y-direction) with respect to the ε_x (strain in the x-direction) are shown in Fig. 2c and Fig. S4a in the SI, respectively. The strains ε_x and ε_y were determined by analysis of images at each stage of the mechanical deformation the films, while ε_z was inferred using the constant volume conditions known to apply for IALCEs. As can be seen in Fig. 2c, all the IALCE films show monotonical deformations in the x–y plane and auxetic responses in the x–z plane. Initially, at low strains, ε_z decreases as ε_x increases, with the film reaching a minimum thickness at ε_{Th}. The film thickness then increases with further strain, recovering to nearly the initial value at higher strains. For the IALCE film polymerized with no applied voltage, the mechanical auxetic threshold strain, ε_{Th} is at $\sim 0.58 \pm 0.05$, in good agreement with previous reports for the same material, and the dark state occurs near that strain.[21] As the voltage applied during polymerization is increased, ε_{Th} is seen to increase, Fig. 2d and Table 1, and the films reach the dark state at slightly higher strains, ε_D. At the highest voltage applied during polymerization, 2.00 V_{rms}, ε_{Th} increases to 0.91 ± 0.05. It can also be seen from Fig. 2c that for the IALCE films polymerized at higher voltages, the maximum thickness that can be achieved during the auxetic response, before the films fail, also decreases slightly as the applied voltage increases.

Table 1 Variation of the auxetic threshold strain with the maximum director angle, θ_{max}, determined by polymerizing the precursor mixture under different applied voltages

Polymerization voltage, V (V_{rms})	0.00	1.05	1.25	1.50	2.00
Maximum director angle, θ_{max} (°)	0	40	60	70	80
Auxetic threshold strain, ε_{Th} (±0.05)	0.58	0.72	0.76	0.83	0.91
Strain for the dark state, ε_D (±0.05)	0.60	0.75	0.80	0.85	0.95

The Poisson's ratio, $\upsilon_{y,z} = d\varepsilon_{y,z}/d\varepsilon_x$ of the films in the x–y and x–z planes respectively can be deduced from the strain-strain data and is shown in Fig. 2d. In calculating the Poisson's ratio, it should be noted that values of true strain, ε_{true} are used, while the simultaneous strains measured are engineering strains ε_{eng}; the two quantities are related by $\varepsilon_{true} = \ln(\varepsilon_{eng} + 1)$. The Poisson's ratio in the x–y plane, υ_y is always positive and takes values ~ 0 at very low strains (Fig. S4), while in the x–z plane, the Poisson's ratio υ_z is ~ 1 at very low strains, and there is a threshold strain beyond which it becomes negative and the system is therefore auxetic. The inset in Fig. 2d shows details around $\upsilon_z = 0$, allowing clear observation of the threshold strain of each film.

Considering the identical T_g for all samples, the tunability of auxetic response must be a consequence of the director patterning within the film. A simple model, described in the SI, can give insight into the dependence of the auxetic threshold on strain for the voltage-patterned films. The model assumes that the Poisson's ratio of an IALCE film with a varying director angle through the thickness can be approximated by finite slices of the IALCE and the bulk Poisson's ratio of the film is then assumed to be the sum of the slices, shown in Fig. S5, calculated for each value of θ_{max}. For the smaller values of θ_{max} ($<60°$), there is an increase in the ε_{Th}, which is qualitatively similar to the experimental observations in Fig. 2d.

However, the increase in the ε_{Th} due to the application of voltage is much greater than is observed experimentally. Additionally for the largest θ_{max} value (80°) an auxetic response is not predicted by the model, though an auxetic response is observed experimentally. The model clearly shows that varying the director profile through the depth of the film will change (increase) the auxetic threshold, though details of the model need to be refined to replicate the exact behaviour. The cyclic mechanical measurement of a planar IALCE sample for 35-cycles over a strain range from 65% to 85% (*i.e.* around the ε_{Th} of the sample), is shown in Fig. 2e. The detailed measurement process is described in the experimental section. Across 35 consecutive cycles, the stress–strain curves gradually converge and stabilize, indicating a progressive reduction in internal dissipation during the initial conditioning cycles. The first cycle exhibits a noticeably higher stress level due to the initial molecular realignment of the mesogenic networks. From the 10th cycle onward, the curves show minimal deviation, suggesting that the material reaches a quasi-steady state with excellent structural resilience. By the 35th cycle, the stress response remains consistent without observable degradation, demonstrating good mechanical durability and cycling stability of the LCE. The performance retention rate of the sample is $\sim 82\%$, with a maximum stress at 0.58 MPa for the 35th cycle and 0.47 MPa for the 1st cycle. The sample after 35-cycles exhibits an auxetic response that is comparable to that of the initial sample, as shown in Fig. S6 in the SI, with no shift of the threshold strain and only a slight change in the magnitude of the auxetic response.

The tunability of the auxetic threshold strain in these chemically identical samples with differently patterned director profiles shows that both the optical and morphological

properties of an IALCE film under strain can be programmed by application of a specific voltage. We can therefore utilize IALCEs as M^{2}ISE materials to realize both 2D optical information and 3D tactile information programming. The following section introduces the design and demonstration of these two properties separately.

3.2. IALCEs for 2D optical M^{2}ISE

3.2.1. The encryption and decryption design. The foundation of using IALCEs as a M^{2}ISE material for 2D optical information is based on the phenomenon that the IALCE film exhibits a dark state under crossed polarizers close to the auxetic threshold strain (seen in Fig. 2b and shown schematically in Fig. 3a).

Applying a voltage during polymerization controls the strain at which dark state appears (Fig. 3b), with specific voltages offering a level of storage and encryption of information, Fig. 3c. Polymerization under selected voltages in the presence of specific exposure masks, allows fabrication of a M^{2}ISE IALCE demonstration with 3-level information storage and encryption in the form of patterns that can be switched between black and white under crossed polarizers. Although the electrodes could themselves be patterned, in this case a single set of electrodes controlled the voltage which was applied to the whole sample, with curing through masks resulting in pixelation. The final 'background' was cured in the isotropic state, achieved by heating the LCE precursor and mold. In the final decryption process, stretching the sample reveals the optical information

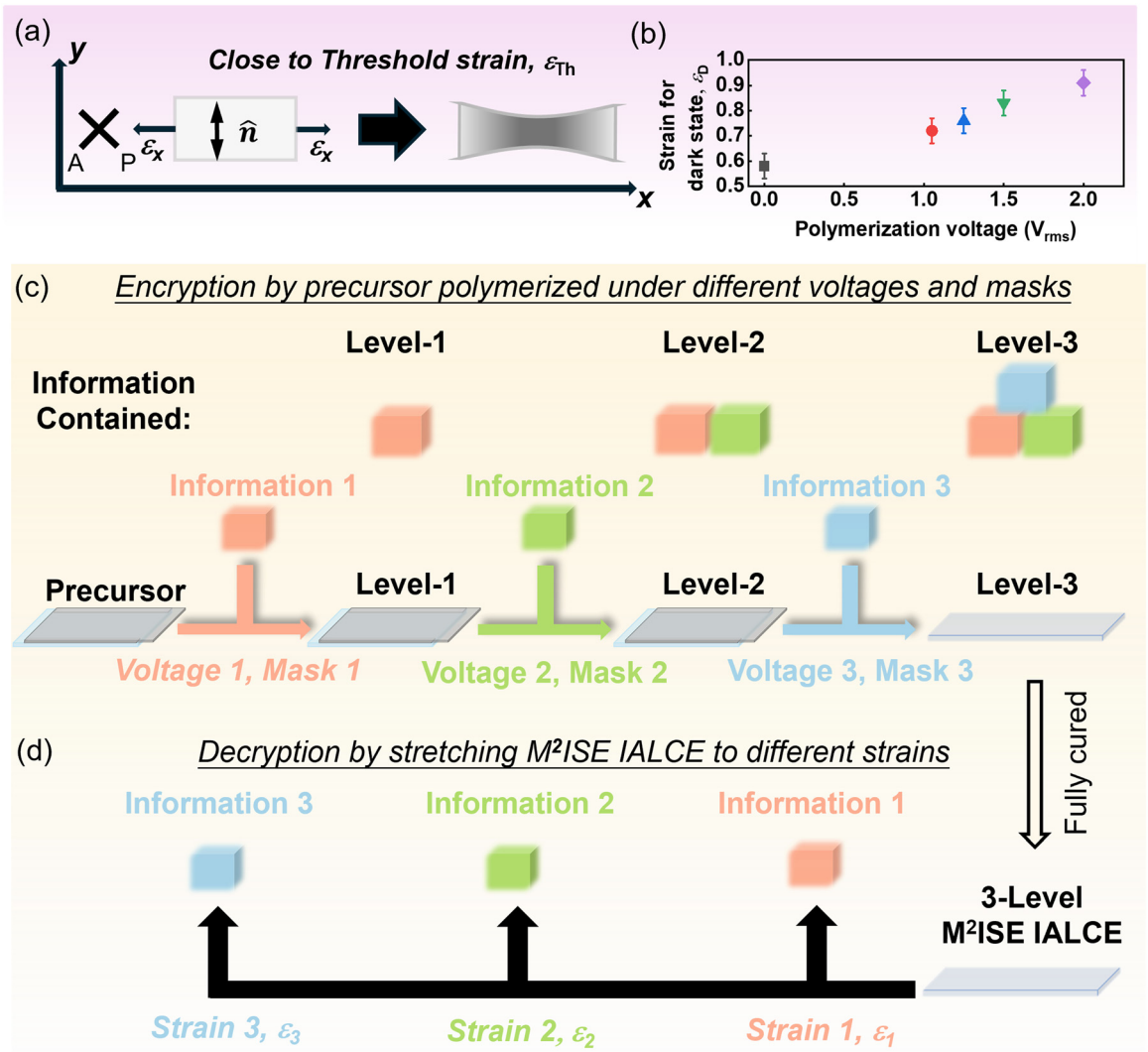

Fig. 3 The encryption design for 2D optical M^{2}ISE IALCEs. (a) The concept diagram showing the optical state change of IALCEs close to the auxetic threshold strain under crossed polarizers. The director is at 45° to the crossed polarizers and the tensile strain is applied along the x-direction. (b) The strains that are necessary to promote the dark state, ε_D, for the various polymerization voltages in this IALCE precursor. (c) The encryption design for 2D optical M^{2}ISE IALCEs. The polymerization is carried out for specific areas of the film exposed by the mask, with different voltages applied sequentially, allowing information 1 to 3 to be coded in optical format. The upper part of the diagram shows the information contained for each level. (d) The decryption design for 2D optical M^{2}ISE IALCEs. During the decryption process, sequential information was revealed by stretching the 3-level M^{2}ISE IALCEs to different strains.

as black under crossed polarizers at the appropriate strain, Fig. 3d.

3.2.2. Fabrication and characterization of 2D Optical M²ISE IALCEs. As a proof-of-concept experiment, we fabricated a 3-level optical information storage and encryption IALCE sample. In this demonstrator, we encrypted the information in the form of a matrix binary signal to improve the information density and make full use of the black-and-white switching characteristics under crossed polarizers. The information content is shown in Fig. 4a with Masks 1, 2 and 3 and voltages of 0 V_{rms}, 1.05 V_{rms} and 1.50 V_{rms}, used to encode the binary sequences: information 1 (000 100 110), information 2 (011 001 000) and information 3 (100 010 001). The main body of the 2D optical M²ISE IALCE sample is synthesized with the precursor in the isotropic phase and deswelling of this region (during the wash-out phase in the fabrication process) causes a dimensional contraction of ~25% in all directions. Consequently, to ensure a circular shape of the patterned area, the patterned region is designed with a width-to-length ratio of ~3 : 2. The isotropic region becomes birefringent (paranematic) with a director oriented largely along the stretching direction under strain, (see video V6 in the SI).[28] Some distortion in the orientation can be seen around the nematic regions at low strains, apparent as birefringent domains, because the strain profile in the film is complicated due to the different elastic moduli of the paranematic and nematic regions. Fig. 4b shows the preparation process of the 2D optical M²ISE IALCE

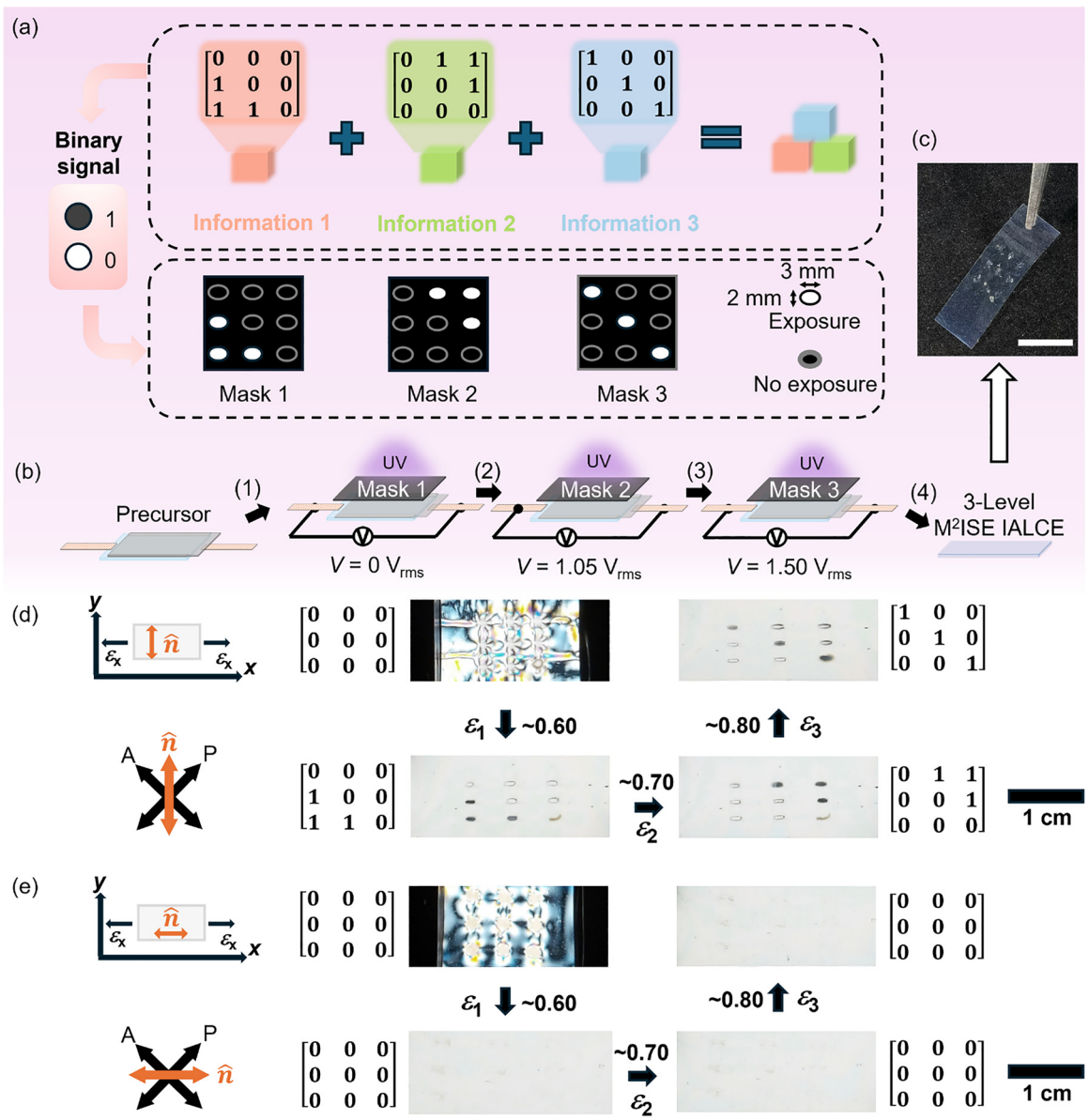

Fig. 4 (a) Optical information in the format of a binary signal, with 3-level information designed into three masks. Black and white represent '1' and '0'. (b) The fabrication process for 2D optical M²ISE IALCEs. (c) A photograph of the IALCE under white light; scale bar is 1 cm. (d) The decryption process with the initial director direction at 45° to the crossed polarizers and perpendicular to the strain. (e) A demonstration of information security; stretching along the initial director direction reveals no information at any strain as there is no auxetic response in this geometry.

Table 2 The strain-dependent display of binary information in the decryption process of 2D optical M^{2}ISE IALCEs measured for the fabricated film

Displayed binary information	(000 100 110)	(011 001 000)	(100 010 001)
Strain (± 0.05)	0.60	0.70	0.80

sample and the actual image of the sample is shown in Fig. 4c. In this work, the patterned domain size macroscopically allows a clearly visible optical signal and a mechanical response that isn't influenced by adjacent strain fields.[65] No field-fringing was observed under electric-field alignment in the low molar mass precursor material. Various patterning strategies exist for fabricating much smaller patterned domains;[66] as the auxetic response is molecular level and it can be on scales of as small as tens of nanometres.[32] Fig. 4d shows the encoded film both schematically and in actual images. The information can be read by holding the film between crossed polarizers with the director at 45° to the polarizer direction and straining perpendicular to the director.

With no strain, the coded parts are bright while the main (isotropic) body exhibits a birefringent pattern due to the strains locked into the system on fabrication. On straining, the main body of the film becomes uniformly bright as the paranematic state is achieved, improving contrast and offering a better display of the decrypted information as it turns black at the desired strain. The whole decryption process, which is entirely consistent with the design, is shown in SI Video S7 and summarized in Table 2. When the sample is strained to ~ 0.60, the first level of information is decrypted and binary information 1 (000 100 110) is displayed in black format in the coded area. Upon straining to ~0.70, the contrast of binary Information 1 decreases and becomes nearly hidden, while binary Information 2 (011 001 000) appears. At a strain of ~0.80, the final level of encrypted binary information (100 010 001) becomes visible, whereas the contrast of all other information decreases to the point of being nearly hidden. These key strains are within the uncertainty quoted for the dark state threshold determined for the unpatterned film (Table 1).

In this system, the security of encrypted information is guaranteed because both the magnitude and direction of the strain are vital decryption elements, which means complete information decryption can only be achieved by stretching the M^{2}ISE IALCE sample in a specific direction to a fixed strain. As a proof-of-concept experiment we stretched a film parallel to the initial director direction, Fig. 4e; no optical information appeared during the entire stretching process. The whole process is shown in SI Video S8. In IALCE systems, auxetic behavior is maintained provided the angle between the loading direction and the director exceeds ~46°.[67] However, when the angle between the loading direction and the director decreases, the auxetic response is affected, with a 0.1 increase in ε_{Th} occurring for a deviation of ~10°. Therefore, straining within ±10° of the optimum direction (perpendicular to the director) would maintain reliable, full information decryption.

3.3. IALCEs for 3D tactile M^{2}ISE

3.3.1. The encryption and decryption design. The auxetic response of a uniform monodomain IALCE film is shown schematically in Fig. 5a (1), manifest as a macroscopic change in thickness. The intrinsic auxetic response is such that the macroscopic thickness change will occur symmetrically, on both sides of the sample. As with in the optical case, the use of an isotropic background increases the display contrast of tactile information (the isotropic region only decreases in thickness on strain while the auxetic region increases). However, including a nematic region in an isotropic film will result in a surface morphology similar to that shown in Fig. 5a (2) caused by both the anisotropic thickness change between the different film areas on deswelling and the shear tension generated between the isotropic and nematic parts of the sample on stretching. Nonetheless, protrusions will emerge at specific strains, allowing the storage of tactile information in the format of Braille haptic letters. Finally, in the design, we note that because the protrusions appear symmetrically on both sides of the film under strain, there is an interesting opportunity to enhance the storage capacity of IALCEs in haptic information applications through vertical flipping and shape symmetry, as will be described later. A Braille haptic letter is generally a set of cylinders with a diameter of ~1.4 mm and a height of ~0.5 mm.[51] In our proof of principle demonstration, the IALCE has a thickness of 100 μm, which is significantly thinner than the height of a unit in a Braille haptic letter, though the auxetic response scales from tens of nanometres to millimetres.[21,32] Potential solutions for realizing the required magnitude of response in Braille letters include the PET-RAFT polymerization,[68] which can increase the sample thickness without altering the auxetic properties, or magnetic field, rather than electric field Fréedericksz alignment which is readily achieved over millimetre thick samples.[69,70]

By choosing appropriate polymerization voltages for the tactile information carrier region, we can achieve height controllable multi-level tactile information storage and encryption. The encryption and decryption designs for a 3-level 3D tactile M^{2}ISE IALCE, using a set of three IALCEs patterned with different voltages, are shown in Fig. 5b and c. The characterization of the IALCE material in Section 2.1 suggests that as the polymerization voltage increases, the auxetic response of the tactile information carrier region will become increasingly delayed (in terms of strain). Upon increasing strain (ε), the patterned regions sequentially emerge, revealing protrusions of different heights (h_1, h_2, h_3), corresponding to both the encoding voltages (V_1, V_2 and V_3) and the applied strain; above the specific auxetic threshold, the heights continue to increase with increasing strain. This sequential emergence of different heights at specific strain levels provides a means for controllable height-based tactile information representation. For this demonstration, each IALCE film was coded with only one letter, so the final step is to arrange the films into a matrix to achieve the desired decrypted Braille haptic information. We produced the design illustrated in Fig. S7 in the SI to encrypt the Braille

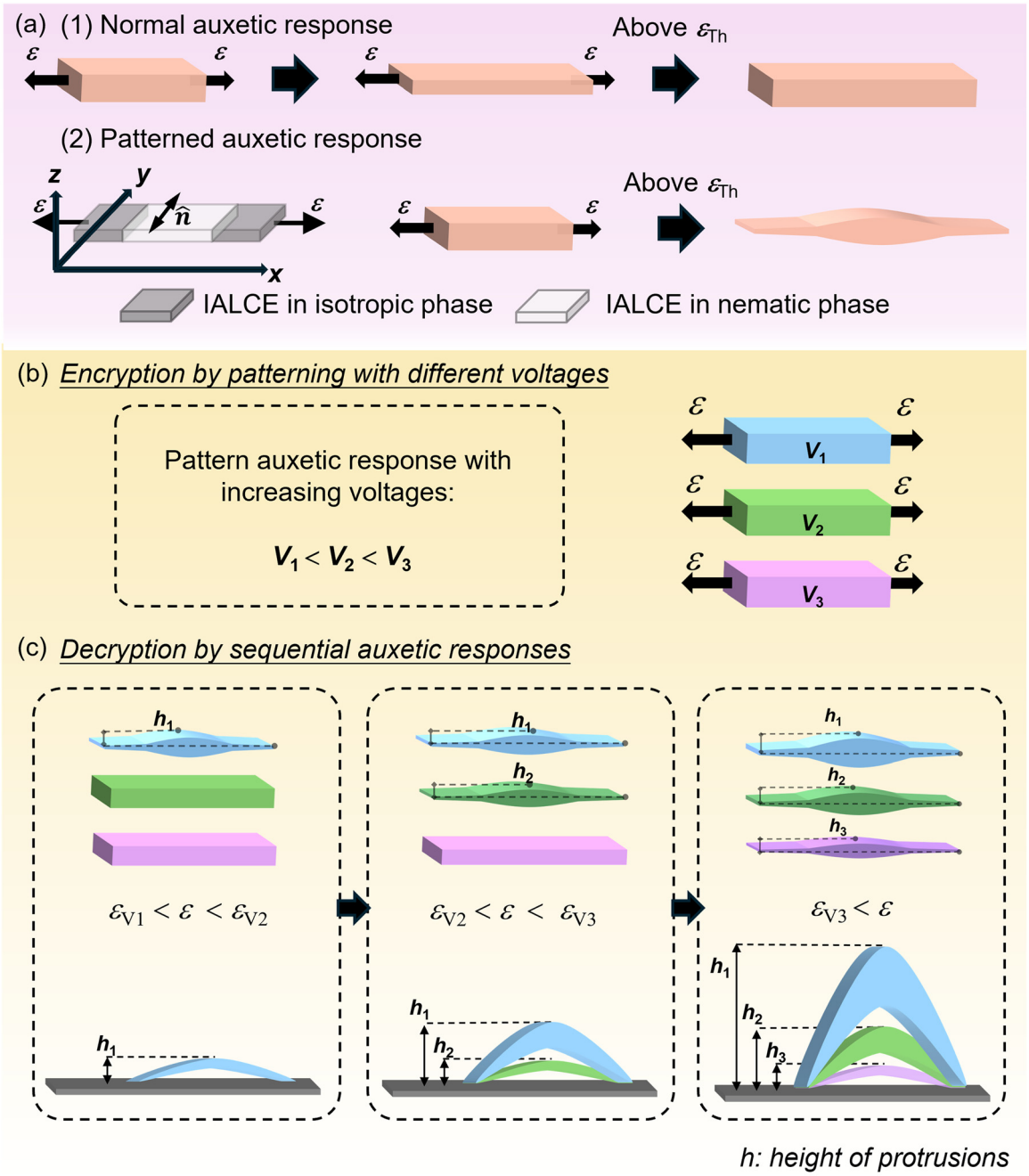

Fig. 5 (a) The morphology changes of (1) a uniform IALCE film and (2) a patterned IALCE region due to the auxetic response. The isotropic part of the film enhances the height protrusion of the nematic region. (b) The encryption design for 3D tactile M^{2}ISE IALCEs. Tactile information is coded into the precursor by patterning the carrier region with different voltages, V_1, V_2 and V_3. (c) The decryption design for 3D tactile M^{2}ISE IALCEs. During the decryption process, sequential tactile information appears on stretching as a protrusion. ε_{V1}, ε_{V2} and ε_{V3} are the auxetic response thresholds corresponding to V_1, V_2 and V_3. h is the height of protrusion and the schematic illustrates that the regions programmed by lower voltages continue to increase in thickness as strain increases.

haptic letters "K", "O", "R" and "W". We make use of the symmetry mentioned earlier to represent the letters "R" and "W", displayed simultaneously on the front and back sides of the same pattern, at the same information level.

3.3.2. Fabrication and characterization of 3D tactile M^{2}ISE IALCEs. As a proof-of-concept experiment, we fabricated a group of 3D tactile M^{2}ISE IALCE films. To achieve better contrast of the height of the surface protrusions, we used an isotropic film which was characterized and compared directly to the patterned nematic films, Fig. S8. During the initial stages of mechanical deformation, the reduction in thickness of isotropic regions occurs more gradually compared to the nematic samples, while the reduction in width is slightly faster (Fig. S8b and c). Once the nematic films begin to exhibit an auxetic response, the

Table 3 The designed strain-dependent display of the Braille haptic letters in the decryption process of 3D tactile M²ISE IALCEs

Displayed braille haptic letters	"K"	"O"	"R"	"W"
Strain range (±0.05)	0.58 to 0.76	0.76 to 0.83	0.83 to 1.00	0.83 to 1.00 (Inversion)

increasingly thin isotropic sample ensures the formation of surface protrusions. To ensure a sufficient strain range for the accumulation of the auxetic response in different protrusions, allowing for effective tactile information display, and to guarantee that there is enough tactile information visible prior to the limit of 1.0 strain, we chose voltages of 0 V_{rms}, 1.25 V_{rms} and 1.50 V_{rms} as V_1, V_2 and V_3 in Fig. S7 with corresponding strains required for the haptic letters shown in Table 3.

Fig. 6a shows a schematic of the fabrication process of 3D tactile M²ISE IALCE films. A real image under white light of the 3D tactile M²ISE IALCEs is shown in Fig. 6b. Fig. 6c illustrates the practical decryption process envisaged for the sequential 3D tactile information generated by the cumulative auxetic deformations. The heights of the protrusions that make up the letters ΔH, measured by laser scanning microscopy, are shown in Fig. 6d. ΔH was obtained by averaging the topological profile with software, "Anytest" and is summarized in Table 4. The measurements are conducted after the staged accumulation of the auxetic responses. For example, the first-stage information, the Braille letter "K" which emerges at strain of

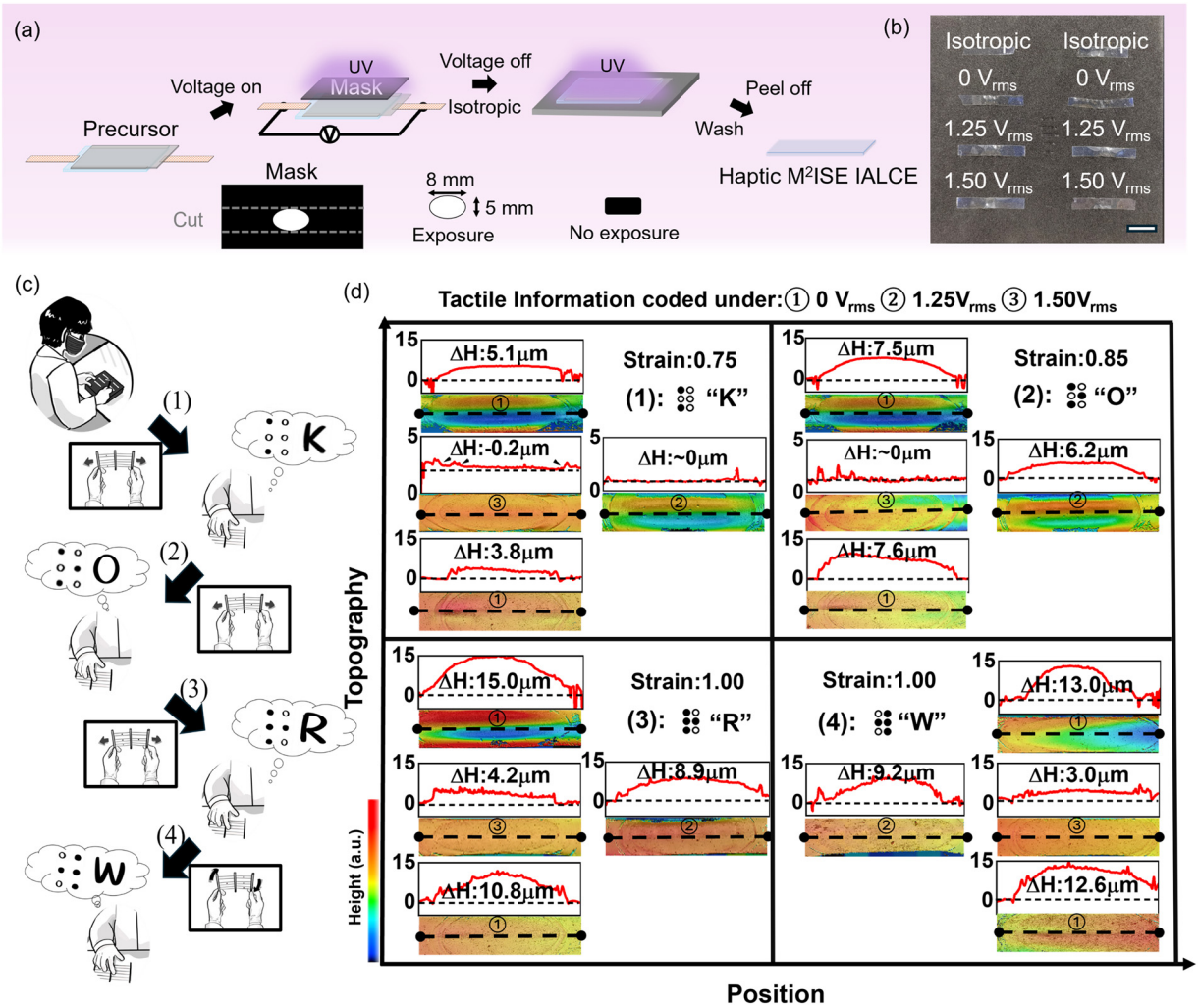

Fig. 6 (a) The fabrication process of a single 3D tactile M²ISE IALCE film. (b) The real image of the 3D tactile M²ISE IALCE films library, including 4 pairs of IALCE films. One pair of strips was prepared in the isotropic phase (and so shows no auxetic behavior) and other 3 pairs are patterned with 0 V_{rms}, 1.25 V_{rms} and 1.50 V_{rms}. The scale bar is 1 cm. (c) The concept schematic using the set of 3D tactile M²ISE IALCEs to reveal the multi-level Braille haptic letters. By stretching (1) $\varepsilon \sim 75\%$, (2) $\varepsilon \sim 85\%$, (3) $\varepsilon \sim 100\%$ and (4) $\varepsilon \sim 100\%$, (Inversion) the Braille haptic letters "K" "O" "R" and "W" appear sequentially. (d) Laser scanning microscopy images of the tactile information included in the films from stages (1)–(4), separately. Numbers 1 to 3 represent the tactile information coded with 0 V_{rms}, 1.25 V_{rms} and 1.50 V_{rms}, respectively. The upper graph in each image shows the height profile measured across the encoded area indicated in the image beneath with the color-height scale shown. ΔH is the measured protrusion height and the dotted line in the upper graph indicates the base line of the ΔH measurement.

$\sim 0.58 \pm 0.05$, is measured at the onset strain of the second stage, around $\sim 0.76 \pm 0.05$; we acquire information at strains of 0.75, 0.85, and 1.00. The POM image of the 3D tactile M^{2}ISE IALCE films at different stages in the mechanical decryption process are shown in Fig. S9, illustrating the dark states in the decryption process which are related to the beginning of the auxetic responses described above. Fig. 6d (1) to (4) correspond to the stages (1)–(4) shown in Fig. 6c. In stages 1–3, the tactile information carrier regions coded at 0 V_{rms} 1.25 V_{rms} and 1.50 V_{rms}, cause the letters K, O and R to sequentially appear under increased strain. The final image (4), shows laser scanning images of the opposite sides of the film with protrusion heights comparable to those in (3), confirming that the intrinsic auxetic response ensures equivalent tactile information on both sides of the film.

We can compare the measured heights of the protrusions with an expected value deduced using the information in Fig. S8d–f. The predicted strain differences ($\Delta\varepsilon_z$) between the nematic and isotropic regions are shown in Table S2 and the predicted protrusion height on each surface (ΔH_e) for a film thickness of 100 μm is included in Table 4. The ''upper sample'' and ''lower sample'' refer to different positions of 0 V-patterned samples within the same haptic pattern, in correlation with Fig. 6d. The data labelled as ''Inversion'' correspond to the protrusion height measured on the opposite surface of the same sample after flipping. For a single film, the protrusions formed on the top and bottom surfaces remain highly symmetric, with consistency of approximately 90%. Throughout the mechanical deformation process of the entire set of films, the height variation of protrusions on each strip closely follows our predictions. It is interesting that the actual heights of the protrusions are in general slightly higher than the expected value. A similar phenomenon was observed by Moorcroft and Raistrick when considering the strain-behavior of a grating embossed in the same IALCE;[32] the amplitude of the grating actually increased on strain due to the auxetic response. And we suggest that such behavior is a consequence of the complex strains at the edges of the protrusions.

Regarding the environmental stability of the decryption of tactile information, it is noted that the auxetic response of the LCE has a small temperature dependence such that the auxetic response occurs at slightly different strains.[57] For this system, a ± 5 °C change from 25 °C causes an approximate ± 0.1 shift in the ε_{Th}, with higher temperatures leading to a lower threshold. The magnitude of the auxetic response is not influenced by temperature below ~ 120 °C for this material. The IALCE system exhibits no swelling in an aqueous environment, *i.e.* for humidity changes from 0% to 100%.[71] As the IALCE is elastomeric, it is also relevant to consider perturbations that may be caused by finger forces. The compression forces are very light during Braille reading and our elastic moduli are comparable to those of other LCEs suggested for Braille.[51,72]

This tactile information storage shares the same information security feature as for optical information, *i.e.* the decryption requires both the magnitude and direction of the strain to work together. However, importantly, unlike the 2D optical M^{2}ISE, the information is displayed in stages, as successive auxetic thresholds are exceeded, rather than as instantaneous changes that occur and then disappear which is the case optically. Thus, the information displayed during the haptic decryption process is cumulative rather than transient. These different M^{2}ISE characteristics make this system unique, coding 2D optical and 3D tactile information in the same sample. The decryption processes for the 2D optical and 3D tactile information do not interfere with each other, which further enhances the security and reliability of the M^{2}ISE function. Moreover, the intrinsic auxetic response of the film expands the dimensions of the mechanical deformation from only one side to both surfaces of the film enhancing the information richness and design flexibility.

4. Conclusions

We have developed a new, facile strategy for realizing M^{2}ISE with IALCEs. To achieve this, a LCE film with auxetic properties was patterned in all three dimensions, so that both optical and haptic information was encoded and revealed at chosen strains.

The specific optical and haptic responses were achieved by imparting pre-determined alignment to the director profile through the depth of a ~ 100 μm thick auxetic LCE film. The desired director orientation was obtained by applying selected voltages, all of which were ≤ 2.00 V_{rms}, to the precursor mixture during polymerization. The maximum angle of the director in the centre of the film was defined by the ratio of the applied voltage to the threshold voltage of the precursor, V/V_{Th}, and determined by fully characterizing the elastic and dielectric properties of the precursor mixture through its Fréedericksz transition. The varying degrees of director alignment through the depth of the films allowed the threshold of the auxetic response to be tuned with threshold strains between $\sim 0.58 \pm 0.05$ and $\sim 0.91 \pm 0.05$.

The auxetic response of an IALCE film involves both the occurrence of a dark state and an increase in thickness beyond specific strains; the voltage-tuneability of the auxetic response

Table 4 The measured (ΔH) and expected (ΔH_e) protrusion height on each surface during decryption process (unit: μm)

	0 V_{rms}-IALCEs (upper sample)		1.25 V_{rms}-IALCEs		1.50 V_{rms}-IALCEs		0 V_{rms}-IALCEs (lower sample)	
ε_x	ΔH	ΔH_e	ΔH	ΔH_e	ΔH	ΔH_e	ΔH	ΔH_e
0.75	5.1	~ 4.0	~ 0	~ 0	-0.2	~ -1	3.8	~ 4.0
0.85	7.5	~ 6.0	6.2	~ 1.5	~ 0	~ 0	7.6	~ 6.0
1.00	15.0	~ 10.5	8.9	~ 3.5	4.2	~ 2.5	10.8	~ 10.5
1.00 (Inversion)	13.0	~ 10.5	9.2	~ 3.5	3.0	~ 2.5	12.6	~ 10.5

therefore allows both the optical and morphological properties of IALCEs to be controlled. Further, because the polymerization process is UV-sensitive, the film can be patterned across its area using masks to define the desired responses in specific areas. Indeed, it is also possible to render regions of the film non-auxetic by polymerizing selected areas at slightly elevated temperatures in the isotropic phase of the precursor mixture. Using these features, we designed and fabricated two types of IALCEs for M^2ISE demonstrations, that separately demonstrated 2D optical and 3D tactile information encoding.

In the case of the 2D optical M^2ISE demonstrator, we intelligently utilized the dark state threshold strain to encode information in a 3 × 3 binary array. The information was encrypted into a single film and decrypted sequentially by applying increasing strain. The fact that decryption requires a specific strain in a particular direction offers two security features. For the 3D tactile M^2ISE demonstrator, haptic information was encoded into patterns within an isotropic (non-auxetic) film background. The height of the protrusion in the patterned auxetic region depended on the voltage applied during patterning, the applied strain and the initial sample thickness. In our demonstration, films were patterned and arranged so that the Braille haptic letters "W", "O", "R" and "K" were sequentially decrypted through strain, making use of the fact that the protrusion emerges on both sides of the patterned regions. In both cases, M^2ISE functionality with three information levels was achieved with the information secured as the decryption factors include both the magnitude and direction of the strain. The decryption processes for the 2D optical information and 3D tactile information do not interfere with each other. This study offers a new approach into the development of M^2ISE soft materials that are easily manufactured and conveniently operated with high safety and versatility.

Author contributions

Y. J. Liu and H. F. Gleeson conceived the research and supervised the project. Z. Wang, T. Raistrick and E. J. Cooper performed experiments and analysed the data. Z. Wang drafted the manuscript. Z. Wang, T. Raistrick and H. F. Gleeson wrote the manuscript. All authors have contributed to the design of the work, analysis of data and given approval to the final version of the manuscript.

Conflicts of interest

HFG holds a position on the board of Auxetec Ltd (Company number 12925662), and HFG and TR are shareholders in Auxetec Ltd.

Data availability

The data that support the findings of this study are available from the University of Leeds at DOI: https://doi.org/10.5518/1665.

Supplementary information (SI) is available. See DOI: https://doi.org/10.1039/d5mh01817j.

Acknowledgements

YJL, MC, MC and ZW acknowledge funding support from the National Key R&D Program of China (Grant 2022YFA1203700); National Natural Science Foundation of China (Grant 62075093); Shenzhen Development and Reform Commission (Grant XMHT20220114005); Shenzhen Science and Technology Innovation Commission (Grant JCYJ20220818100413030); High Level of Special Funds from Southern University of Science and Technology (Grants G030230001 and G03034K004); Graduate Education Innovation Grants from Southern University of Science and Technology (Grant 202401002). ZW acknowledges part-support from the University of Leeds. TR and HFG acknowledge funding from the Engineering and Physical Sciences Research Council, UK, Grant EP/V054724/1. The authors thank Ms Yingtong Wen (tungbabe@163.com) for drawing Fig. 6c of this manuscript. The authors thank Prof. Shaolin Xu from Southern University of Science and Technology for the use of the equipment-Laser Scanning Microscope.

References

1 K. Li, J. Wang, W. Cai, H. He, M. Cen, J. Liu, D. Luo, Q. Mu, D. Gerard and Y. J. Liu, *Nano Lett.*, 2021, **21**, 7183–7190.
2 H.-L. Wang, H.-F. Ma and T.-J. Cui, *Adv. Sci.*, 2022, **9**, 2204333.
3 J. Wang, K. Li, H. He, W. Cai, J. Liu, Z. Yin, Q. Mu, V. K. S. Hisao, D. Gérard, D. Luo, G. Li and Y. J. Liu, *Laser Photonics Rev.*, 2022, **16**, 2100396.
4 H. Huang, H. Li, J. Yin, K. Gu, J. Guo and C. Wang, *Adv. Mater.*, 2023, **35**, 22111117.
5 B. Liu, C.-L. Yuan, H.-L. Hu, H. Wang, Y.-W. Zhu, P.-Z. Sun, Z.-Y. Li, Z.-G. Zheng and Q. Li, *Nat. Commun.*, 2022, **13**, 2712.
6 H. Li, M. Zhu, F. Tian, W. Hua, J. Guo and C. Wang, *Chem. Eng. J.*, 2021, **426**, 130683.
7 H. Zeng, Z. He, Y. Wu, S. Gao, F. Mao, H. Fan, X. Fan, W. Kan, Y. Zhu, H. Zhang and B. Assouar, *Adv. Funct. Mater.*, 2024, **34**, 2405132.
8 G. Qu, W. Yang, Q. Song, Y. Liu, C.-W. Qiu, J. Han, D.-P. Tsai and S. Xiao, *Nat. Commun.*, 2020, **11**, 5484.
9 X. Guo, J. Zhong, B. Li, S. Qi, Y. Li, P. Li, D. Wen, S. Liu, B. Wei and J. Zhao, *Adv. Mater.*, 2021, **34**, 2103192.
10 Z. Yu, K. Zhao, Y. Zhao, M. Wu, B. Cheng, R. Qian, S. Chen and C. Ye, *J. Mater. Chem. C*, 2023, **47**, 16527–16535.
11 Q. Wang, Z. Qi, Q.-M. Wang, M. Chen, B. Lin and D.-H. Qu, *Adv. Funct. Mater.*, 2022, **32**, 2208865.
12 Z. Quan, Q. Zhang, H. Li, S. Sun and Y. Xu, *Coord. Chem. Rev.*, 2023, **493**, 215287.
13 Y. Xie, X. Zhao, H. Wang, Y. Tian, C. Liu, J. Wu, J. Cui, Z. Zhou, J. Chen and X. Chen, *Angew. Chem., Int. Ed.*, 2024, **137**, e202414846.

14 T. H. Ware, M. E. Mcconney, J. J. Wie, V. P. Tondiglia and T. J. White, *Science*, 2015, **347**, 982–984.
15 T. J. White and D. J. Broer, *Nat. Mater.*, 2015, **14**, 1087–1098.
16 N. Qian, H. K. Bisoyi, M. Wang, S. Huang, Z. Liu, X.-M. Chen, J. Hu, H. Yang and Q. Li, *Adv. Funct. Mater.*, 2023, **33**, 2214205.
17 R. Lan, J. Sun, C. Shen, R. Huang, Z. Zhang, L. Zhang, L. Wang and H. Yang, *Adv. Mater.*, 2020, **32**, 1906319.
18 Q. He, Z. Wang, Y. Wang, A. Minori, M. T. Tolley and S. Cai, *Sci. Adv.*, 2019, **5**, eaax5746.
19 J. Wang, H. Zhou, Y. Fan, W. Hou, T. Zhao, Z. Hu, E. Shi and J.-A. Lv, *Mater. Horiz.*, 2024, **11**, 1877–1888.
20 D. Mistry, S. D. Connell, S. L. Mickthwaite, P. B. Morgan, J. H. Clamp and H. F. Gleeson, *Nat. Commun.*, 2018, **9**, 5095.
21 Z. Wang, T. Raistrick, A. Street, M. Reynolds, Y. J. Liu and H. F. Gleeson, *Materials*, 2023, **16**, 393.
22 M. Cheng, H. Zeng, Y. Li, J. Liu, D. Luo, A. Priimagi and Y. J. Liu, *Adv. Sci.*, 2021, **9**, 2103090.
23 J. Yang, H. Zhang, A. Berdin, W. Hu and H. Zeng, *Adv. Sci.*, 2023, **10**, 2206752.
24 Y. Chen, C. Valenzuela, X. Zhang, X. Yang, L. Wang and W. Feng, *Nat. Commun.*, 2023, **14**, 3036.
25 Z. Deng, H. Zhang, A. Priimagi and H. Zeng, *Adv. Mater.*, 2022, **36**, 2209683.
26 K. Dradrach, M. Zmyślony, Z. Deng, A. Priimagi, J. Biggins and P. Wasylczyk, *Nat. Commun.*, 2023, **14**, 1877.
27 H. Guo, A. Priimagi and H. Zeng, *Adv. Funct. Mater.*, 2021, **32**, 2108919.
28 D. Mistry, M. Nikkhou, T. Raistrick, M. Hussain, E. I. L. Jull, D. L. Baker and H. F. Gleeson, *Macromolecules*, 2020, **53**, 3709–3718.
29 C. Ohm, M. Brehmer and R. Zentel, *Adv. Mater.*, 2010, **22**, 3366–3387.
30 J. Liu, H. Zeng, M. Cheng, Z. Wang, J. Wang, M. Cen, D. Luo, A. Priimagi and Y. J. Liu, *Mater. Horiz.*, 2021, **9**, 942–951.
31 M. Cheng, W. Cai, Z. Wang, L. Chen, D. Yuan, Z. Ma, Z. Bai, D. Kong, M. Cen, S. Xu, A. K. Srivastava and Y. J. Liu, *ACS Appl. Mater. Interfaces*, 2024, **16**, 31776–31787.
32 T. Moorhouse and T. Raistrick, *Adv. Opt. Mater.*, 2024, **12**, 2400866.
33 L. Chen, J. Liu, M. Cheng, Z. Wang, W. Cai, Z. Ma, Z. Bai, D. Kong, M. Cen and Y. J. Liu, *Opt. Express*, 2024, **32**, 12528–12536.
34 J. Bai, L. Zhang, Z. Shi and X. Jiang, *Adv. Funct. Mater.*, 2023, **33**, 2212556.
35 J.-B. Hou, X.-S. Chen and Y. Zhao, *Adv. Funct. Mater.*, 2024, **34**, 2314510.
36 X. Wang, K. Yang, B. Zhao and J. Deng, *Small*, 2024, **20**, 2404576.
37 X. Sang, A. Khan, R. Xu, K. Zhang, Y. Tian, Y. Li, M. Feng, L. Liu, F. Song and W. Huang, *Adv. Opt. Mater.*, 2024, **12**, 2400064.
38 L. Yu, B. Chen, Z. Li, Q. Huang, K. He, Y. Su, Z. Han, Y. Zhou, X. Zhu, D. Yan and R. Dong, *Chem. Soc. Rev.*, 2023, **52**, 1529–1548.
39 M. Schwartz, G. Lenzini, Y. Geng, P. B. Ronne, P. Y. A. Ryan and J. P. F. Lagerwall, *Adv. Mater.*, 2018, **30**, 1707382.
40 Y. Geng, R. Kizhakidathazhath and J. P. F. Lagerwall, *Adv. Funct. Mater.*, 2021, **31**, 2100399.
41 S. H. Choi, J. H. Kim, J. Ahn, T. Kim, Y. Jung, D. Won, J. Bang, K. R. Pyun, S. Jeong, H. Kim, Y. G. Kim and S. H. Ko, *Nat. Mater.*, 2024, **23**, 834–843.
42 H.-Q. Wang, Y. Tang, Z.-Y. Huang, F.-Z. Wang, P.-F. Qiu, X. Zhang, C.-H. Li and Q. Li, *Angew. Chem., Int. Ed.*, 2023, **62**, e202313728.
43 J. Gao, Y. He, X. Cong, H. Yi and J. Guo, *ACS Appl. Mater. Interfaces*, 2022, **14**, 53348–53358.
44 J. Gao, M. Tian, Y. He, H. Yi and J. Guo, *Adv. Funct. Mater.*, 2022, **32**, 2107145.
45 Z.-Y. Xu, L. Li, X. Yin, L.-Y. Shi, K.-K. Yang and Y.-Z. Wang, *Adv. Mater. Technol.*, 2024, **9**, 2302009.
46 S. Zhang, C. Sun, J. Zhang, S. Qin, J. Liu, Y. Ren, L. Zhang, W. Hu, H. Yang and D. Yang, *Adv. Funct. Mater.*, 2023, **33**, 2305364.
47 J.-X. Yang, X.-L. Zhang, L. Yin, J. Jiang, T. Liu, J.-Y. Liu, Z.-T. Xu, H.-Y. Bai, H.-W. Ma, Y. Zhao, Y. Li and L. Han, *Chem. Eng. J.*, 2025, **507**, 160312.
48 Y. Zhai, Z. Wang, K.-S. Kwon, S. Cai, D. J. Lipomi and T. N. Ng, *Adv. Mater.*, 2021, **33**, 2002541.
49 T. Ohzono, M. O. Saed, Y. Yue, Y. Norikane and E. M. Terentjev, *Adv. Mater. Interfaces*, 2020, **7**, 1901996.
50 N. Torras, K. E. Zinoviev, J. Esteve and A. Sánchez-Ferrer, *J. Mater. Chem. C*, 2013, **1**, 5183.
51 A. Gablier and E. M. Terentjev, *Nano Select*, 2023, **4**, 324–332.
52 M. Shinohara, Y. Shimizu and A. Mochizuki, *IEEE Trans. Rehabil. Eng.*, 1998, **6**, 249–256.
53 D. Leithinger, S. Follmer, A. Olwal and H. Ishii, *IEEE Comput. Graphics Appl.*, 2015, **35**, 5–11.
54 W. Yang, J. Huang, R. Wang, W. Zhang, H. Liu and J. Xiao, *IEEE Trans. Haptics*, 2021, **14**, 712–721.
55 I. Hwang, S. Mun, J.-H. Youn, H. J. Kim, S. K. Park, M. Choi, T. J. Kang, Q. Pei and S. Yun, *Nat. Commun.*, 2024, **15**, 2554.
56 A. Richter and G. Paschew, *Adv. Mater.*, 2009, **21**, 979–983.
57 T. Raistrick, M. Reynolds, E. J. Cooper, J. Hobbs, V. Reshetnyak and H. F. Gleeson, *Soft Matter*, 2025, **21**, 8849–8866.
58 T. Raistrick, Z. Zhang, D. Mistry, J. Mattsson and H. F. Gleeson, *Phys. Rev. Res.*, 2021, **3**, 023191.
59 E. J. Cooper, M. Reynolds, T. Raistrick, S. R. Berrow, E. I. L. Jull, V. Reshetnyak, D. Mistry and H. F. Gleeson, *Macromolecules*, 2024, **57**, 2030–2038.
60 D. Mistry, P. B. Morgan, J. H. Clamp and H. F. Gleeson, *Soft Matter*, 2018, **14**, 1301–1310.
61 S. R. Berrow, T. Raistrick, R. J. Mandle and H. F. Gleeson, *Polymers*, 2024, **16**, 1957.
62 S. R. Berrow, T. Raistrick, R. J. Mandle and H. F. Gleeson, *ACS Appl. Polym. Mater.*, 2025, **7**, 4517–4524.
63 G. Vertogen and W. H. De Jeu, *Thermotropic Liquid Crystals Fundamentals*, Springer Science & Business Media, Berlin, Germany, 2012.
64 D. Mistry, PhD thesis, University of Leeds, 2018.
65 T. H. Ware, J. S. Biggins, A. F. Shick, M. Warner and T. J. White, *Nat. Commun.*, 2016, **7**, 10781.
66 Z. Wang, M. Cheng, Z. Wu, Y. Qiu and Y. Liu, *Chin. J. Liq. Cryst. Disp.*, 2024, **1**, 1–20.
67 D. Mistry and H. F. Gleeson, *J. Polym. Sci. Pol. Phys.*, 2019, **57**, 1367–1377.

68 S. R. Berrow, R. J. Mandle, T. Raistrick, M. Reynolds and H. F. Gleeson, *Macromolecules*, 2024, **57**, 5218–5229.
69 J. A. Herman, R. Telles, C. C. Cook, S. C. Leguizamon, J. A. Lewis, B. Kaehr, T. J. White and D. J. Roach, *Adv. Mater.*, 2024, **36**, 2414209.
70 R. Mouhoubi, V. Lapinte and S. Blanquer, *Adv. Funct. Mater.*, 2025, **35**, 2424400.
71 E. J. Cooper, PhD thesis, University of Leeds, 2025.
72 M. Etezad, R. Joshi and F. L. Cibrian, *Displays*, 2025, **90**, 103133.